JOURNAL OF MATERIALS SCIENCE: MATERIALS IN MEDICINE **11** (2000) 837–845

Reliability of Pd based dental alloys regarding to corrosion resistance and production processes

M.R. PINASCO[1], E. ANGELINI[2], E. CORDANO[1], E. MAGI[1], F. ROSALBINO[2]
[1]Dip. di Chimica e Chimica Ind., Università di Genova, Via Dodecaneso 31, 16146 Genova, Italia
E-mail: metal@chimica.unige.it
[2]Dip. di Scienze dei Materiali e Ing. Chimica, Politecnico di Torino, Corso Duca degli Abruzzi 24, 10129 Torino, Italia
E-mail: angelini@polito.it

The knowledge of the relationship among chemical composition, microstructure, productive processes, functional properties, quality and price of the final product is an ever greater requirement for the firms producing dental alloys as well as for the dental laboratories making prosthesis.

The present study deals with the evaluation of the corrosion resistance of high-Pd and Pd-Ag alloys by quantification of released ions following the recent European regulations suggested. Moreover the reliability of the alloys as far as concern their corrosion resistance was also investigated in relation to the different steps of alloy industrial production and restoration forming processes as well as after homogenization treatments followed by different cooling rate.

The very complex microstructure of both alloys was greatly affected by the different casting conditions, deformation rate and thermal treatments used in alloy industrial production and prosthesis manufacturing. However the corrosion resistance of both alloys remained very good in all metallurgical states. The potentiodynamic tests allowed to distinguish among the structural conditions: the homogenization treatments, eliminating segregation inside the different phases, improved further the corrosion resistance of both alloys.

1. Introduction

The manufactures of dental alloys are particularly concerned with obtaining products with the various concomitant characteristics necessary. Some of these properties depend on the requirements to facilitate alloy industrial production or prosthesis forming and on the working processes in the dental laboratory; others are necessary to make the product suitable to perform its functions in the oral cavity. So the material must have proper mechanical properties, wear resistance, hardness, toughness to withstand daily masticatory stress; it must show appropriate aesthetic qualities, it is essential that the material must be biocompatible and therefore it must have high corrosion resistance, to be neither toxic nor irritating. Biocompatibility and corrosion resistance of the alloys are strictly connected because their toxicity depends on the quality and the quantity of the released ions, on the eventual synergic or antagonist effects and on the length of time they remain in contact with organic tissues [1–6].

Noble metals and, particularly, Au based alloys have always been preferred for their high chemical stability, however the high cost of row materials is also of great importance and has led to the formulation of less noble alloys and to the substitution of gold with palladium. Recently the relative fluctuation of the price of the noble metals originated a new problem. Moreover, severe European regulations regarding biomaterials impose more and more restricted limits to the quality of products and manufacturing processes. The knowledge of the relationships between chemical composition, structural state, functional properties, productive process, quality and price of the finished product is an ever greater requirement for the firms producing biomaterials. Moreover dental technicians have to know how much the certified alloy will maintain its properties after having suffered the suitable processes to give the right shape and aesthetic requirements to restoration.

The present study belongs to a wider research (carried out in collaboration with a manufacturer), aimed at the formulation of precious metal dental alloys and at their optimization taking into consideration the previously discussed requirements. The composition and the structural features of the alloys were put in relation to their corrosion resistance in different environments, to control their reliability also in relation to the alloy production and prosthesis forming processes.

TABLE I Nominal composition (wt%) of Alloy A and B

	Alloy A (nobility 58.7)							Alloy B (nobility 81)				
	Pd	Ag	Sn	In	Zn	Ru		Pd	Cu	Ga	Au	Ge
wt%	57.8	30.1	6	4	X	*	wt%	79	9.5	9	2	*

*Indicates ''element in trace;'' X indicates ''wt% ≤ 2.''

2. Experimental details

The analyzed materials were a high-Pd alloy with high nobility and a Pd-Ag based alloy with mean nobility, which are used for the forming of prosthesis for ceramic veneering (manufacturer Puppo Iori & C). Their nominal composition is listed in Table I.

The alloys were examined in the metallurgical conditions representing every step from industrial production (as cast and cold rolled) to the forming of the restoration (after recasting with the lost wax technique and heat treatments for ceramic firing). To enhance the knowledge of the influence of segregation phenomena on alloy corrosion behavior, a part of the as cast material was homogenized for 15 h at 940 °C for Alloy A and at 900 °C for Alloy B. Afterwards samples of both alloys were quenched in a mixture of water and ice and others were allowed to cool in the switched off furnace. Every metallurgical state was characterized by means of optical and electron scanning microscopy (SE and BSE) before and after etching with a freshly prepared aqueous solution of $(NH_4)_2S_2O_8$ (10%) and NaCN (10%), EDS microanalysis and XR-diffraction.

The corrosion behavior of the alloys under study was evaluated by means of potentiodynamic anodic polarization curves recorded in Ringer's solution (NaCl 9.00 g; $NaHCO_3$ 0.20 g; KCl 0.43 g; $CaCl_2$ 0.24 g; distilled water up to 1 dm^3) at room temperature; the potential scan started from the free corrosion potential (E_{corr}) to $+1200$ mV versus a saturated calomel electrode (SCE), at a scan rate $dE/dt = 0.25$ mV/s. The electrochemical cell was constituted by a Pyrex beaker with an airtight cover, containing in addition to the sample a Pt counterelectrode and a reference electrode. All measurements were performed with a Solartron mod. 1286 electrochemical interface connected to an IBM PS2 computer. The corrosion resistance of samples of both alloys, prepared according to the methods of prosthesis manufacturing, was tested by static immersion following the directives imposed by recent proposal of European regulations. Five samples for each alloy were immersed for a week in an aqueous solution of NaCl 0.1 M and of lactic acid 0.1 M at the temperature of 37 ° ± 1 °C. After the test the solutions were analyzed without any dilution by ICP emission atomic spectrometry (Jobin Yvon 24) provided with an ultrasonic nebulizer. The working conditions are reported in Table II. In Table III the wavelengths (nm) for the analysis of each element are listed.

TABLE II Working conditions for ICP-AES analysis

Condenser temp.	2 °C
Heater temp.	140 °C
Ar coating flow	0.7 l/min
Ar plasma flow	14.0 l/min
Ar aerosol flow	0.6 l/min
Power	800 W
Sample rate	2.0 ml/min

The surface of all tested samples was examined by SEM.

3. Results and discussion

3.1. Structural characterization

The microstructure of both alloys is characterized by the presence of many phases and several structural features. This complexity is caused by the great number of components in both the alloys and by the alloying of the principal elements (Pd, Ag) with Ga, In, Sn, Zn and Ge, which leads to the formation of various intermediate phases already in the binary equilibrium phase-diagrams [7]. Moreover the structural complexity is increased by the off-equilibrium conditions, deriving from the industrial production processes and working conditions as a dental prosthesis, which cause segregation and heterogeneity inside the different phases.

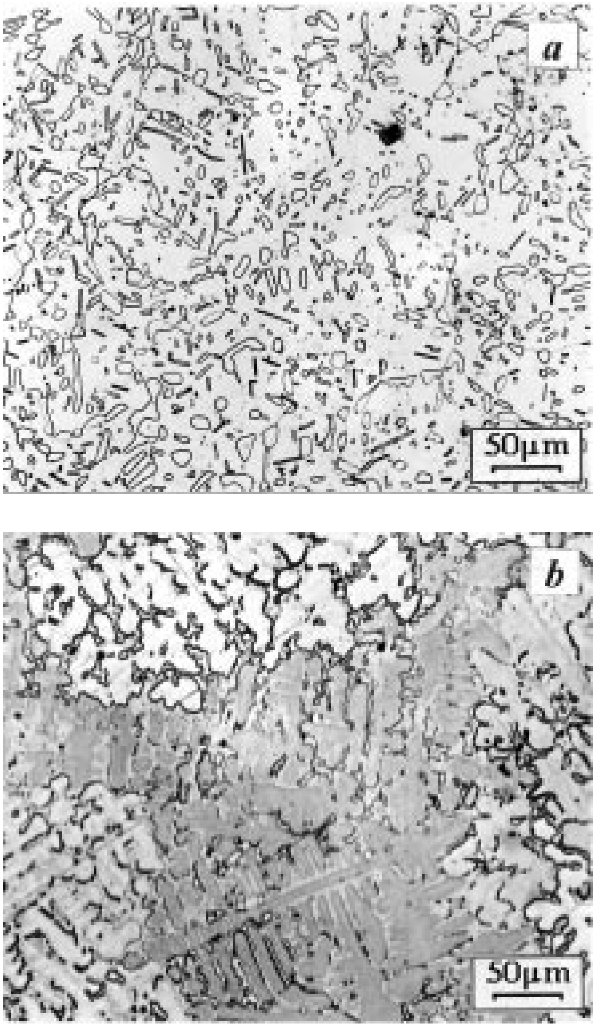

Figure 1 (a,b) Microstructure (OM) of Alloy B after homogenization and quenching (a) and in the as cast condition (b).

TABLE III Wave lengths (nm) and detection limits (ppb) for the analysis of each element

Element	Pd	Au	Ag	Cu	Zn	Sn	In	Ga	Ge	Ru
λ(nm)	340.458	242.795	328.068	324.754	213.856	189.989	230.606	294.364	209.426	240.272
d.l. (ppb)	10	5	4	9	134	52	12	20	36	14

TABLE IV Phases identified in every metallurgical state by XR-diffraction

Metallurgical state	Phases detected	
	Alloy A	Alloy B
Homogenized and quenched	f.c.c. b.c.t.	f.c.c. f.c.t. primitive cubic
Homogenized and slowly cooled	f.c.c. b.c.t.	f.c.c. orth. Pd_2Ga-type primitive cubic
As cast	f.c.c.	f.c.c. f.c.t.(I) f.c.t.(II) primitive cubic
Recast and heat treated	f.c.c. b.c.t.	f.c.c. f.c.t. orth. Pd_2Ga-type primitive cubic

The material after 15 h homogenization and quenching in water and ice presented the ''simpler'' structure for both alloys (Fig. 1a). The homogenization eliminated the primary heterogeneity, quite evident in the as cast material, and the high cooling rate deleted the solid state transformations below the quenching temperature (Fig. 1b). In the microstructure of both the alloys two phases can be distinguished: a matrix and another phase, appearing darker by SEM-SE observation (Fig. 2a). This phase is present in grains with rounded joints along the matrix grain boundaries and in rods which are rectangular, acicular or more rounded, inside the grains of the matrix. Since DTA measurements indicate that Alloy A solidifies monophasic, the darker phase should be generated by a solid state transformation. The same assertions are not valid for Alloy B, because DTA measurements revealed that not only one phase originates from the liquid. The composition of the phases is reported in Figs 3a and 4a. In Alloy B the matrix is enriched in Pd while the darker phase is richer in Cu. In Alloy A the matrix is impoverished in Pd and quite enriched in Ag to reach a ratio Ag:Pd equal to 1:1, Sn and In concentrate in the darker phase. By XR-diffraction two phases (f.c.c. and b.c.t.) were detected in Alloy A, as shown in Table IV [8]. Differently in Alloy B, X-ray diffraction pointed out three phases (f.c.c., primitive cubic and f.c.t.) in this metallurgical state. We hypothesized that the tetragonal structure might be a coherent distortion of the f.c.c. matrix, therefore not visible by optical and scanning electron microscopy. The analysis allowed us to attribute the f.c.c. structure to the matrix in both alloys, the b.c.t. structure to the darker phase of Alloy A and the primitive cubic structure to the darker phase of Alloy B.

The cooling in the furnace after the stay at high temperature allows the development of solid state transformations and the microstructure of both the alloys becomes more complex. Moreover the phases morphologically corresponding to those found in the homogenized and quenched material have a different composition and ratios between the alloying elements. In Alloy A (Fig. 2b) the matrix was the seat of a precipitation. The precipitates are small in size and are often not yet well distinguishable from the parent matrix. The darker phase is richer in Pd and Sn and poorer in Ag compared to that of the homogenized and quenched material (Fig. 3b). Next to it lamellar nodules and a new massive phase formed, appearing grey by SEM-SE observation, with a very different composition. However X-ray diffraction showed the presence of the same two phases already detected in the homogenized and quenched alloy. Both the phases of the homogenized and quenched Alloy B are involved in solid state reactions, giving rise to several structural features: in

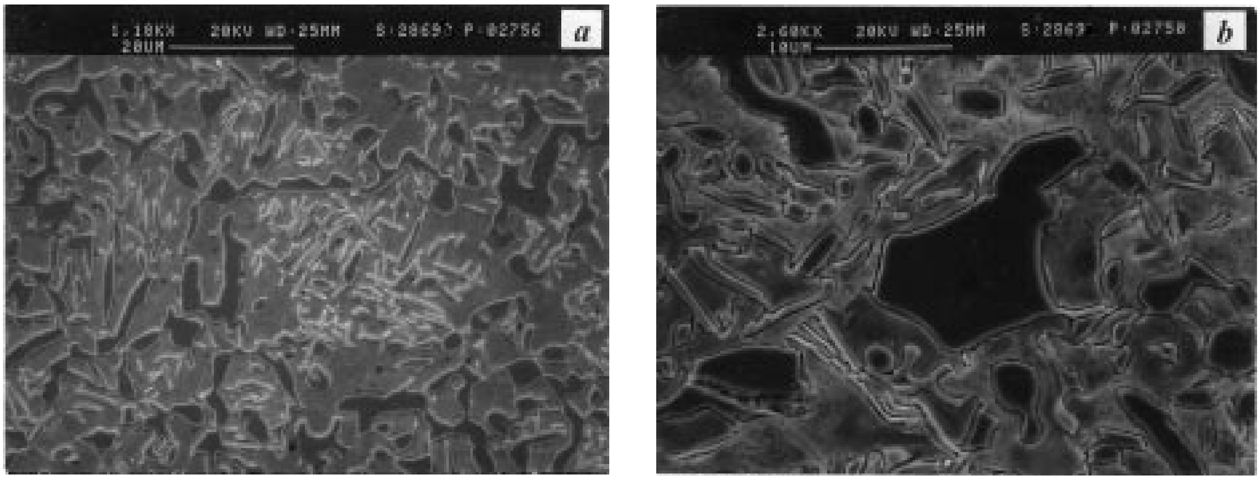

Figure 2 (a,b) (SEM-SE) Alloy A homogenized and quenched (a) and homogenized and slowly cooled (b).

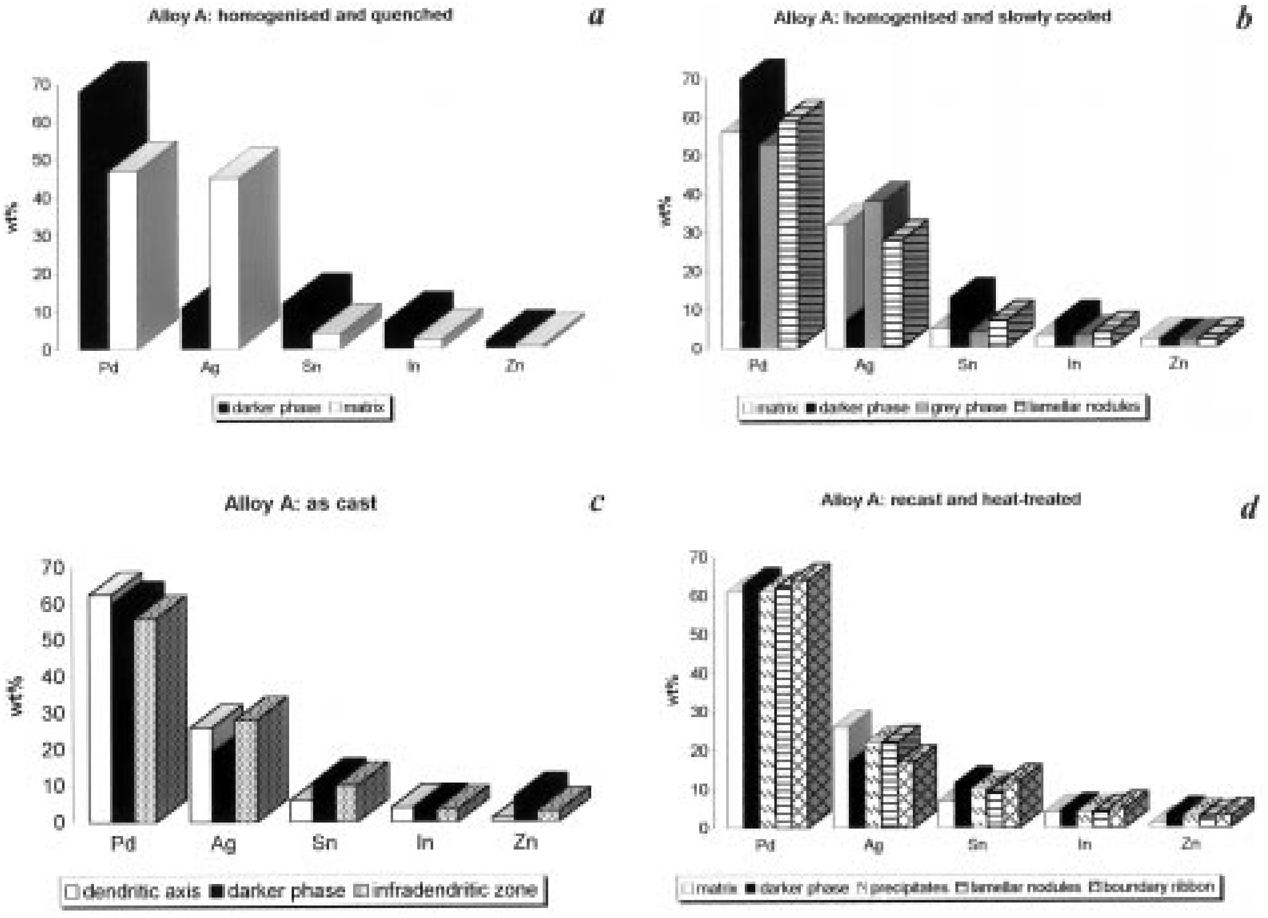

Figure 3 (a,b,c,d) Alloy A: composition (wt %; EDS analysis) of the principal structural features evidenced in every metallurgical state.

the matrix small needle-like precipitates, crossing with particular angles, originated because of continuous precipitation. In the grains of the darker phases, lengthened lamellae with Widmanstätten or feather-like morphology appeared. Besides lamellar nodules are also present. Fig 4b shows the mean composition of the principal structural constituents; it is evident that the amount of Ga is greater in the lengthened lamellae, while Cu concentrates in the darker phase. XRD patterns also show evidence of transformations taking place: the f.c.t. phase of the homogenized and quenched material disappeared and a new orthorhombic Pd_2Ga-based phase appeared. The f.c.c. and the primitive cubic are again present.

It was not always possible to make a correlation between a particular microstructural aspect and a crystal structure detected by XRD because the EDS analysis of some phases are complicated by their small size. Moreover every microstructural feature is a solid solution with a certain compositional range containing all the alloying elements in different percentage.

The microstructure of both the alloys is strongly influenced by the solidification conditions, which lead to a different rate of segregation and to various dimensions of the structural constituents. The size of primary grains increases from the as cast alloy to the recast with the lost wax technique material (subsequently heat-treated according to the manners of the ceramic firing). The cooling rate up to room temperature and the chemical heterogeneity have a synergic effect on the kind of solid state transformation and on its progression rate. So the number of the present phases, their size, their composition and their morphology change in the different metallurgical states examined.

Alloy A as cast showed a different distribution of the alloying elements (Fig. 3c): the central zone of the dendritic axis was richer in Pd while the infradendritic zone contained a greater amount of Ag, Sn and Zn. There was also a different transformation rate, in fact in the infradendritic zone secondary phases (acicular precipitates, lamellar nodules and the darker phase) already formed, while the center of the dendritic axis did not yet appear to be transformed (Fig. 5a). However XRD analysis revealed only the f.c.c. solid solution, probably for the low quantity, small size and dispersion of the secondary phases.

The strong segregation of Alloy B as cast (Fig. 1b) was the cause of the different kinds of transformation of the center of the dendritic axis and of the contiguous infradendritic zone: in the former a very fine globular precipitation was present and in the latter parallel striations, the microstructural appearance characterizing the f.c.t. AuCuI type structure [9–11], were visible. Other microstructural constituents were lamellar nodules and the darker phase, strongly enriched in Ga and Ge, compared to the matrix (Fig. 4c). X-ray diffraction detected the predominant f.c.c. solid solution, the primitive cubic, in a small amount, and two f.c.t. phases, one already identified in the homogenized and quenched material and the other identified only in this metallurgical state, probably for the heavy non-equilibrium conditions (Table IV).

Heat treatments simulating ceramic firing do not

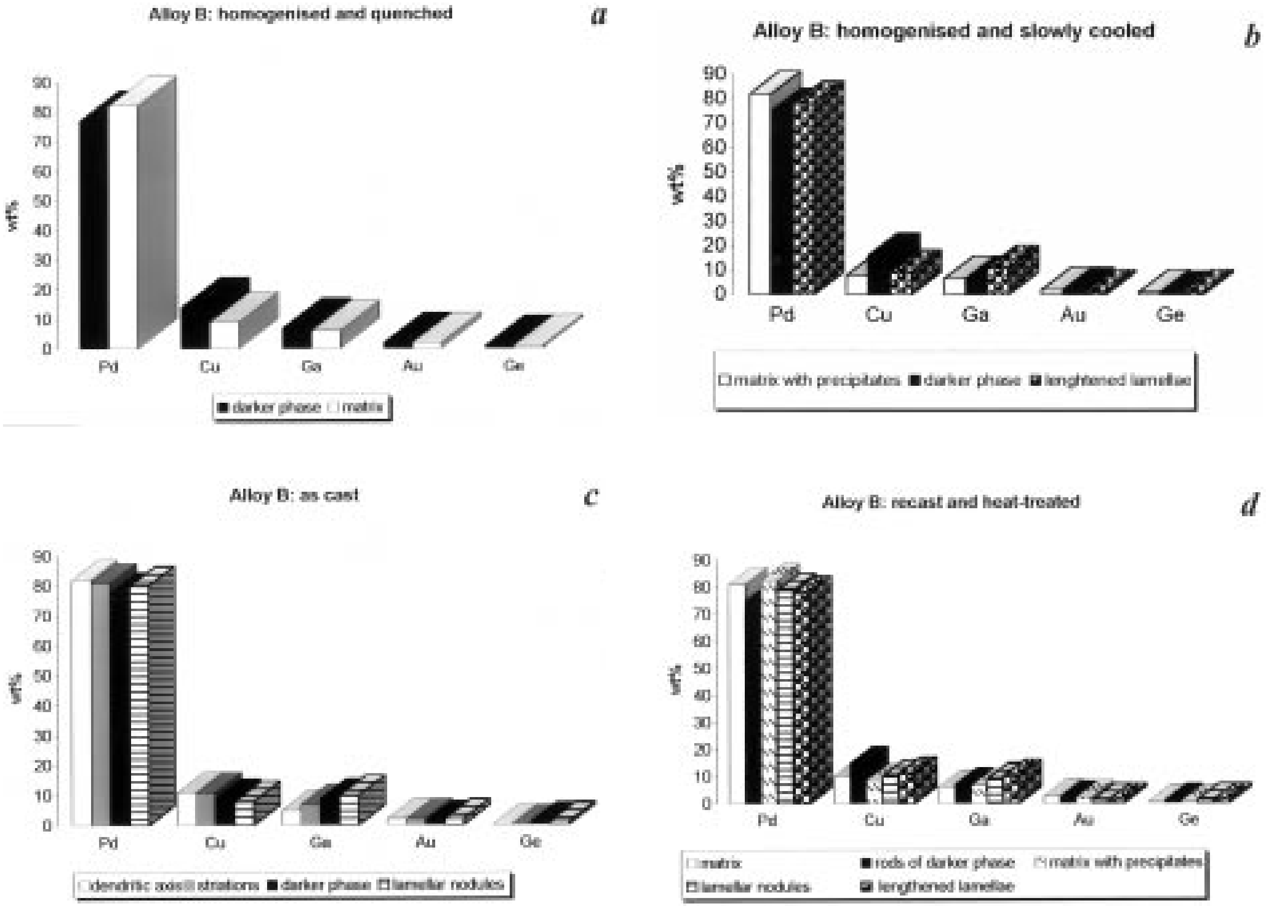

Figure 4 (a,b,c,d) Alloy B: composition (wt %; EDS analysis) of the principal structural features evidenced in every metallurgical state.

eliminate the solidification heterogeneity. In the recast and heat-treated alloys a compositional difference and a different transformation rate between the dendritic axis and the infradendritic zone, the latter being more greatly transformed, was quite evident.

In Alloy A (Fig. 6a) the lamellar nodules and the precipitates already seen in the as cast and in the homogenized and slowly cooled material can be observed, but the precipitates had a bigger and more defined size. Most of the islands of the darker phase appeared to be in the process of transformation, probably due to a precipitation with a different mechanism: discontinuous (formation of lamellar nodules) and continuous (precipitates inside a lamella). The grain boundary was constituted by a phase in shape of ribbon. In this phase, in the grains of the darker phase and in the derived structural constituents, Pd, Sn and Zn were concentrated, while the greatest amount of Ag was in the matrix; on the whole it is possible to note that the tendency of Ag content is opposite to the one for Pd and Sn (Fig. 3d). Also in this metallurgical state XR diffraction detected the same two phases: f.c.c. and b.c.t.

In the infradendritic zone of Alloy B (Fig. 7a) the same

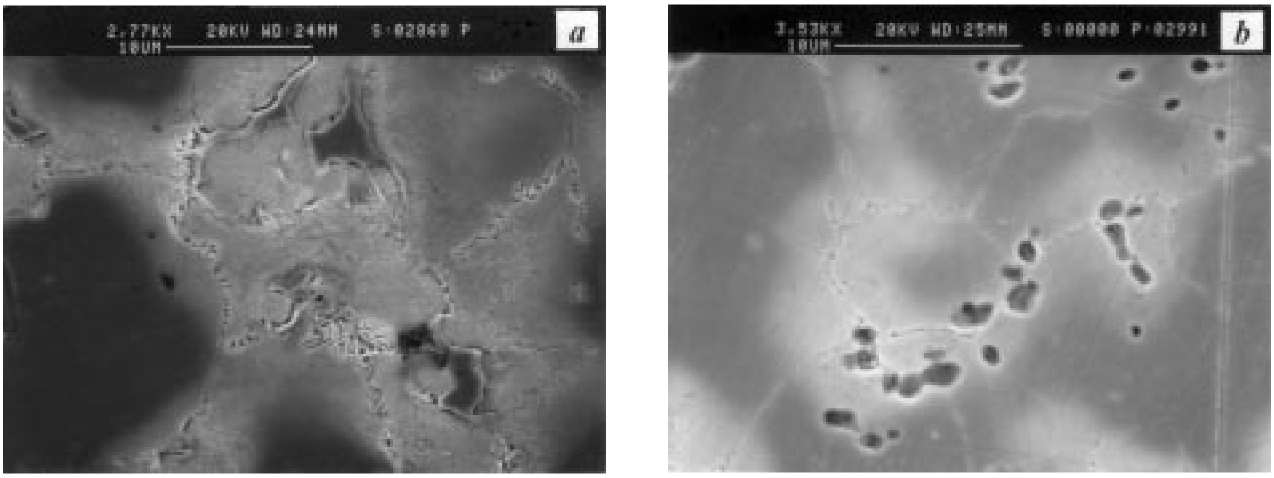

Figure 5 (a,b) (SEM-SE) Alloy A as cast before (*a*) and after electrochemical test plus light metallographic etching (*b*).

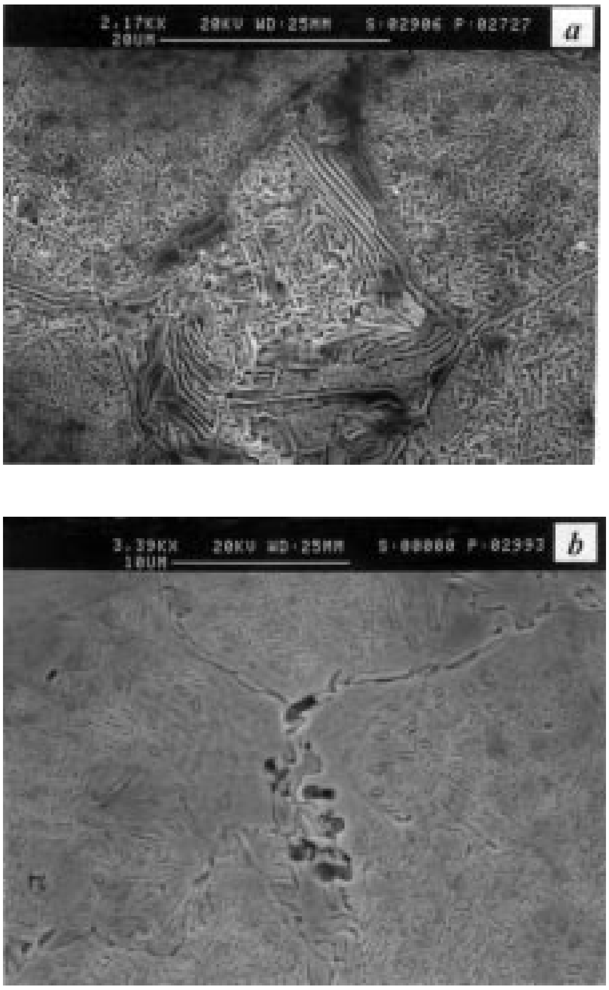

Figure 6 (a,b) (SEM-SE) Alloy A simulating veneering treatments before (a) and after electrochemical test plus light metallographic etching (b).

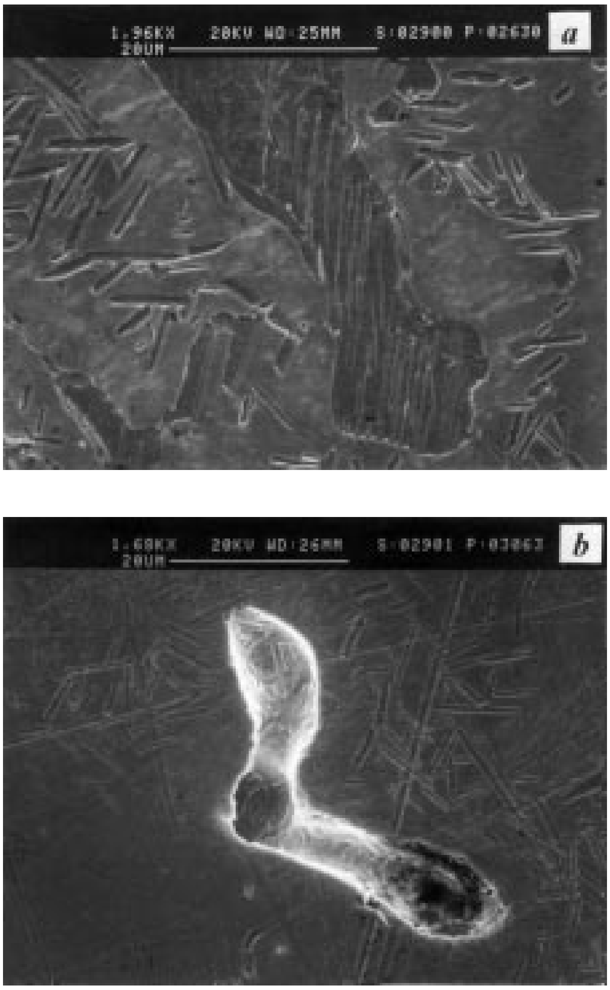

Figure 7 (a,b) (SEM-SE) Alloy B simulating veneering treatments before (a) and after electrochemical test plus light metallographic etching (b).

structural aspects of the homogenized and slowly cooled material can be found: needle-like precipitates, grains of the darker phase with the stocky and lengthened lamellae and the thin lamellar nodules. Rods of the untransformed darker phase, similar for its morphology and composition to that of the homogenized and quenched material, surrounded the untransformed dendritic axis, separating this zone from the one covered by the needle-like precipitates. The Pd amount is greater in the matrix of the dendritic axis and in the zone with the needle-like precipitates; Cu concentrates in the darker phase and Ga in the lengthened lamellae inside the grains of the transformed darker phase (Fig. 4d). XR-diffraction showed the presence of four phases: the f.c.c. solid solution, the primitive cubic, the Pd_2Ga-like orthorhombic and the f.c.t.

Cold rolling (without any intermediate recrystallization treatments) until a deformation rate of 85–90% makes the as cast structure of both the alloys quite fibrous. The secondary phases found in the infradendritic zone and at the grain boundary of the as cast alloy were shattered and lengthened in the direction of the cold-rolling. In Alloy B the state of the fibers has a ''lozenge''-like morphology (Fig. 8), characterizing the gold alloys with copper [9, 12] in analogous rates of deformation, although Au amount is only 2% wt. The fibers in Alloy A, completely lacking in Au and Cu, do not show this morphology.

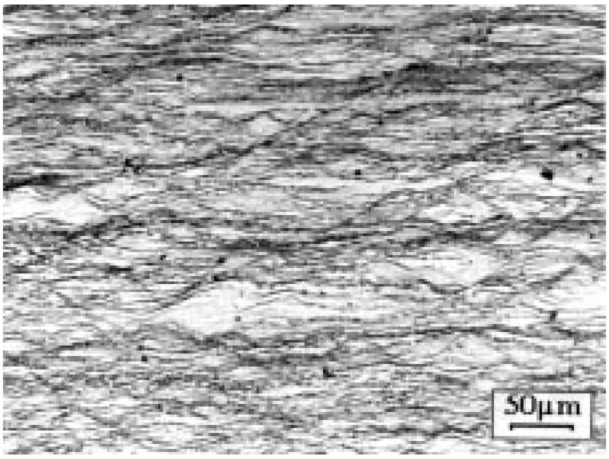

Figure 8 Microstructure (OM) of cold rolled Alloy B (85–90% deformation rate).

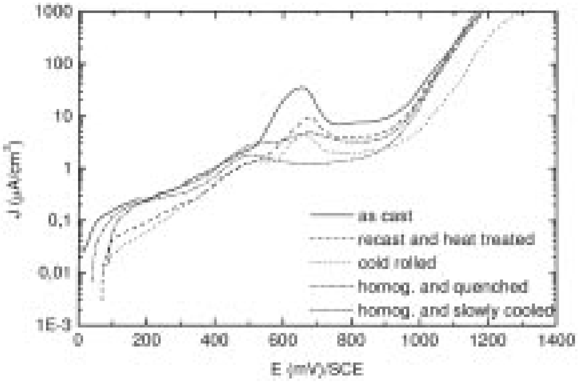

Figure 9 Anodic polarization curves recorded in Ringer's solution on Alloy A in the different metallurgical states examined.

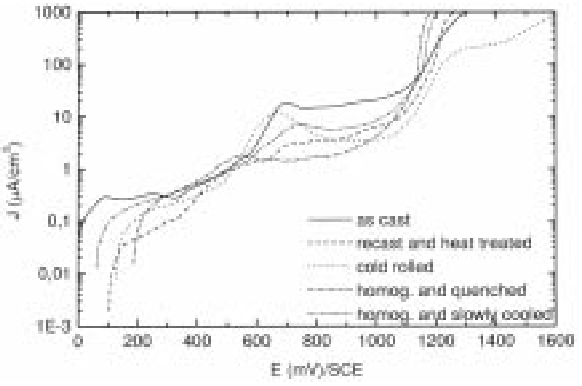

Figure 10 Anodic polarization curves recorded in Ringer's solution on Alloy B in the different metallurgical states examined.

3.2. Corrosion behavior

3.2.1. Electrochemical tests

Fig. 9 shows the anodic polarization curves recorded in Ringer's solution on Alloy A. The free corrosion potential ranges between $+10\,\text{mV}$ (SCE) for the as cast material and $+80\,\text{mV}$ (SCE) for the homogenized and quenched one; the shapes of the curves are similar for all the examined metallurgical states and are characterized by very low current densities, $\leq 1\,\mu\text{A/cm}^2$, starting from the free corrosion potential up to $+900\,\text{mV}$ (SCE), followed by an increase at higher potentials. Alloy A as cast exhibits an activation peak at $+650\,\text{mV}$ (SCE), corresponding to the anodic oxidation of silver through the reaction: $\text{Ag} + \text{Cl}^- \Rightarrow \text{AgCl} + \text{e}^-$ [13], which is responsible for the increase of the anodic current density; the same peak is also shown by the recast and heat treated samples and the cold rolled ones, but the corresponding current density values are considerably lower. As evidenced in Fig. 9, no activation peak is observed in the case of the homogenized and quenched alloy and the homogenized and slowly cooled one, the latter characterized by the better corrosion behavior showing anodic current density values $\leq 1\,\mu\text{A/cm}^2$ in a wide potential range. All the polarization curves show a sharp increase in the current density at anodic potentials higher than $+900\,\text{mV}$ (SCE), connected to the oxygen evolution reaction:

$$4\ \text{OH}^- \rightarrow 2\text{H}_2\text{O} + \text{O}_2 + 4\ \text{e}^-$$

After the potenziodynamic tests the surface of all samples appeared weakly corroded. The superficial modifications caused by the potenziodynamic test are identifiable with round gathered cavities. A light metallographic etching with $(\text{NH}_4)_2\text{S}_2\text{O}_8$ (10%) and NaCN (10%), always distinguishable from the effects of the electrochemical tests, shows that in the as cast alloy, the cavities started forming at the grain boundaries (Fig. 5*b*) between the matrix and the darker phase, which is richer in Sn, Zn and In. The average EDS analysis of the whole surface of the as cast alloy changed after the electrochemical tests: Cl was present, In and Zn halved, Pd decreased and Ag and Sn increased. Corrosion products are visible on the surface, mainly constituted by AgCl and SnClO_x, according to the EDS analysis.

For the other metallurgical states, SEM observations showed that the corrosive attack is lower than in the as cast alloy, supporting the results of the curves, and the cavities are more rare and are smaller in size. In the homogenized material, both water-quenched and slowly cooled, the cavities are again located at the grain boundary between the matrix and the darker phase, but no corrosion products are present on the surface. Concerning the recast and heat treated samples, the cavities are connected to the ribbon-shaped phase, constituting the grain boundary, richer again in Sn and Zn.

In Fig. 10 the anodic polarization curves of Alloy B recorded in Ringer's solution are reported. In this case the free corrosion potential values are higher than those of Alloy A and the range between $+60\,\text{mV}$ (SCE) for the homogenized and slowly cooled samples and $+180\,\text{mV}$ (SCE) for the quenched ones. The shape of the polarization curves is similar in all the metallurgical states and characterized by very low current densities, $\leq 1\,\mu\text{A/cm}^2$, starting from the free corrosion potential up to $+500\,\text{mV}$ (SCE); above this value the as cast alloy shows the highest current density value, about $20\,\mu\text{A/cm}^2$, followed by the cold rolled one, $10\,\mu\text{A/cm}^2$, and by the quenched one, $5\,\mu\text{A/cm}^2$. As for Alloy A, the better corrosion behavior is shown by the homogenized and slowly cooled material, characterized by current density values lower than $1\,\mu\text{A/cm}^2$ in a wide potential range, extending up to $+1000\,\text{mV}$ (SCE). The sharp increase in the anodic current density shown by the polarization curves at potentials higher than $+1100\,\text{mV}$ (SCE) is connected to the oxygen evolution reaction.

SEM observation of the surface of all the metallurgical states after potenziodynamic tests showed that the corrosive attack appears as a few round cavities small in size; no corrosion products, but spots lighter than the surrounding zones were visible. A light metallographic etching with $(\text{NH}_4)_2\text{S}_2\text{O}_8$ (10%) and NaCN (10%) and SEM-BSE vision made it possible to evidence that these cavities were located in the secondary grains where a poliphasic structure, constituted by the darker phase plus the stocky and lengthened lamellae, is present (Fig. 7*b*).

The above results allow us to affirm that both the alloys under study show a satisfactory corrosion resistance independently of their chemical composition and their metallurgical state. The good corrosion behavior is also evidenced by the very low anodic current density values, $< 1\,\mu\text{A/cm}^2$, recorded in the potential range of interest in the oral cavity, $-100 \div +300\,\text{mV}$ (SCE) [14]. Within this good

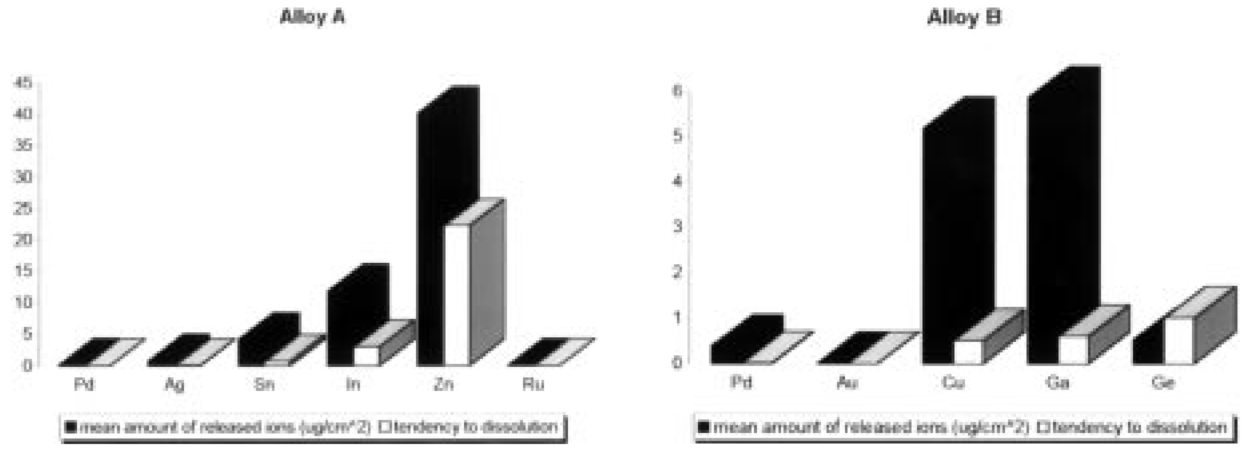

Figure 11 Ion-release from Alloy A (right) and Alloy B (left) in the metallurgical conditions characterizing the prosthesis in the oral cavity.

corrosion resistance the high sensibility of the potenziodynamic tests allows to distinguish the different tendency to anodic dissolution of every examined metallurgical state: the homogenization treatment, eliminating segregation inside the different phases, has induced an improvement in corrosion resistance of both tested alloys.

3.2.2. Static immersion tests

Five samples for each alloy were tested. The detection limits (ppb) for each analyzed element, regarding to the test solutions without any dilution, are listed in Table III. The mean standard deviation (of the instrument) was less than 3%.

The results of the analysis of Alloy A and Alloy B are reported in Fig. 11. The dark histogram indicates the mean amount of the dissolved ions in $\mu g/cm^2$ for each element; in the light one every value is carried to the corresponding weight percentage, as indicated in the nominal composition.

The nominal mean quantity of dissolved ions per cm^2 of exposed surface is 57 $\mu g/cm^2$ for Alloy A and 12 $\mu g/cm^2$ for Alloy B. These values are lower than the maximum limit of 100 $\mu g/cm^2$ imposed by the European regulations.

The total variation coefficient, taking into account the preparation of the samples (from the sampling to the final analytical measurement) naturally proved to be quite high: 68% for Alloy A and 54% for Alloy B. Nevertheless the global ranges of concentration of the total quantity of the dissolved ions remain below the upper limit imposed by the European regulations: Alloy A $18 \div 96\ \mu g/cm^2$, Alloy B $5.4 \div 18.3\ \mu g/cm^2$.

As was predictable, the noble metals (Pd and Au) release the smallest amount of ions independently of their weight percentage. For Alloy B the smallest concentration is that of Au, followed by that of Pd, of Ge, of Cu and finally that of Ga. Analogously for Alloy A the smallest concentration is that of Ru, followed by that of Pd and by those of the non-noble metals.

Comparing the data of Pd, the only metal common to the two alloys, it is worthwhile noting that, besides nobility, also the alloying, as already highlighted [15], is another factor influencing the ion release, in fact the larger quantity of Pd is released by Alloy B, even though its nobility is greater.

Making the ratio between the amount ($\mu g/cm^2$) of the ions released by each element and its nominal percentage, it is possible to express better the tendency to dissolution for each metal. From these data we can observe that Ge, although it is the less abundant element of Alloy B, has the greater tendency to dissolution and it is followed by Ga and Cu; this tendency for Pd and Au is less than three orders of magnitude. The examination of this tendency for the constituents of Alloy A pointed out that also for Alloy A the relation with the metal nobility is respected: Pd has the smallest tendency to dissolution, while for Zn and In this tendency is much higher than those of the other alloying elements. Considering the data obtained for both the alloys it is possible to schematise the tendency to dissolution of the examined elements:

$$Zn > In > Ge > Sn > Ga > Cu > Ru > Ag > Pd > Au$$

After the test, the visual examination showed no superficial changes for either of the alloys. SEM observation revealed a few zones of weak localized attack characterized mainly by an erosion and partly by the formation of thin films. The zones of superficial alteration are localized around shrinkage microcavities, but in a few cases they might be related to the removal of secondary phases.

EDS analysis revealed a little alteration of the superficial layers, albeit insignificant, in agreement with the small amount of the released ions.

4. Conclusions

- The microstructure of both alloys is very complex and characterized by the presence of many phases. The microstructural state of both alloys is greatly influenced either by the various steps of alloy industrial production processes or by prosthesis manufacturing (recasting and heat treatments as in ceramic firing). The structural complexity is increased by the off-equilibrium conditions, causing segregation and heterogeneity inside the different phases and changes in their number and composition. Although Alloy A has on the whole a structure less complicated than Alloy B, both the alloys show several microstructural features. In Alloy A by XRD analysis, two phases at most were identified. In Alloy B the microstructural changes are also shown by the variations of the number and of the kinds of crystalline structures.

- In spite of the dependence of the microstructure of the alloys towards productive processes, both alloys exhibit a satisfactory corrosion resistance in all metallurgical states, thus showing their reliability, when every operation of prosthesis manufacturing is carried out correctly.
- The good electrochemical behavior of the alloys is evidenced by the very low anodic current density values recorded in the potential range of interest in the oral cavity $-100 \div +300\,\mathrm{mV}$ (SCE). However, the high sensitivity of the electrochemical tests allows us to observe the slight differences in the corrosion rates and to relate them to the presence of phases that are more or less prone to corrosive attack.
- The alloys in the metallurgical condition representing the prosthesis in the oral cavity show their great corrosion resistance also by the static immersion tests. The total amount of the dissolved ions per cm^2 of exposed surface is less than the upper limit of $100\,\mu\mathrm{g/cm}^2$ for both alloys. Alloy B, which is the most noble, releases less ions than Alloy A. As was predictable, the noble metals (Pd and Au) release the smallest amount of ions, but the alloying is another influencing factor. Considering the data obtained for both the alloys it is possible to schematize the tendency to dissolution of the examined elements:

$$\mathrm{Zn} > \mathrm{In} > \mathrm{Ge} > \mathrm{Sn} > \mathrm{Ga} > \mathrm{Cu} > \mathrm{Ru} > \mathrm{Ag} > \mathrm{Pd} > \mathrm{Au}$$

Acknowledgments

Puppo Iori & Co., Genoa, Italy, and in particular Dr. P.M. Bovone, is gratefully acknowledged for the production and the supply of the examined alloys. This research was financially supported by CNR (PFMSTA II- Sott. Biomateriali) and by MURST, Rome, Italy.

References

1. J. C. WATAHA, R. G. CRAIG and C. T. HANKS, *J. Dent. Res.* **70** (1991) 45.
2. J. C. WATAHA, C. T. HANKS and R. G. CRAIG, *J. Biomed. Dent. Res.* **28** (1994) 427.
3. P. L. FOGLIO BONDA, *Il Dentista Moderno*, **8** (1997) 59.
4. H. F. HILDEBRAND, J. C. HORNEZ and N. SPATH, Proceedings of 3rd European Precious Metals Conference, Florence, September 1997, 1.
5. M. SCHUSTER, Proceedings of 3rd European Precious Metals Conference, Florence, September 1997, 67.
6. K. ENDO, K. MATSUDA and M. OHNO, *Corrosion Engineering* **42** (1993) 913.
7. T. MASSALSKI, H. OKAMOTO, P. R. SUBRAMANIAN and L. KACPRZAK eds., ''Binary alloy phase diagrams II ed.'' (ASM Int. 1990).
8. M. R. PINASCO, E. CORDANO and M. GIOVANNINI, *J. Alloys Comp.* **289** (1999) 289.
9. E. STAGNO, M. R. PINASCO and M. G. IENCO, *Prakt. Met.* **20** (1983) 433.
10. K. YASUDA and K. HISATSUNE, *Gold Bull.* **26** (1993) 50.
11. M. R. PINASCO, M. G. IENCO, E. STAGNO and R. GRIMALDI, Proceedings Noble Metals Fabrication and Technology Seminar, Jerusalem, April 27–May 5 (1985) 47.
12. E. STAGNO and M. R. PINASCO, *Mémoires Scientifiques Révue Métallurgie* **75** (1978) 529.
13. K. ENDO, Y. ARAKI, I. KAWASHIMA, Y. YAMANE, H. OHNO and K. MATSUDA, *Higashi Nippon Dental Journal* **8** (1989) 49.
14. G. J. EWERS and E. H. GREENER, *J. Oral. Rehab.* **12** (1985) 469.
15. E. ANGELINI, P. PICCARDO, M. R. PINASCO and F. ROSALBINO, *Metall. Ital.*, **90** (1998) 25.

Received 8 July 1999
and accepted 19 November 1999